



# AMERICAN METEOROLOGICAL SOCIETY

*Journal of Hydrometeorology*

## **EARLY ONLINE RELEASE**

This is a preliminary PDF of the author-produced manuscript that has been peer-reviewed and accepted for publication. Since it is being posted so soon after acceptance, it has not yet been copyedited, formatted, or processed by AMS Publications. This preliminary version of the manuscript may be downloaded, distributed, and cited, but please be aware that there will be visual differences and possibly some content differences between this version and the final published version.

The DOI for this manuscript is doi: [10.1175/2010JHM1272.1](https://doi.org/10.1175/2010JHM1272.1)

The final published version of this manuscript will replace the preliminary version at the above DOI once it is available.



**Understanding the daily cycle of evapotranspiration: a method to  
quantify the influence of forcings and feedbacks**

CHIEL C. VAN HEERWAARDEN \* AND JORDI VILÀ-GUERAU DE ARELLANO

*Meteorology and Air Quality Section, Wageningen University, The Netherlands*

AMANDA GOUNOU, FRANÇOISE GUICHARD AND FLEUR COUVREUX

*CNRM-GAME, Météo-France and CNRS, Toulouse, France*

\* *Corresponding author address:* Chiel C. van Heerwaarden, Wageningen University, PO BOX 47, 6700

AA Wageningen, The Netherlands

E-mail: chiel.vanheerwaarden@wur.nl

## ABSTRACT

A method to analyze the daily cycle of evapotranspiration over land is presented. It quantifies the influence of external forcings, such as radiation and advection, and of internal feedbacks induced by boundary-layer, surface-layer and land surface processes on evapotranspiration. It consists of a budget equation for evapotranspiration that is derived by combining a time derivative of the Penman-Monteith equation with a mixed-layer model for the convective boundary-layer.

Measurements and model results of days in two contrasting locations are analyzed using the method: mid-latitudes (Cabauw, The Netherlands) and semi-arid (Niamey, Niger). The analysis shows that the time evolution of evapotranspiration is a complex interplay of forcings and feedbacks. Although evapotranspiration is initiated by radiation, it is significantly regulated by the atmospheric boundary-layer and the land surface throughout the day. Boundary-layer feedbacks enhance in both cases the evapotranspiration up to  $20 \text{ W m}^{-2} \text{ h}^{-1}$ . However, in the case of Niamey this is offset by the land surface feedbacks, since the soil drying reaches  $-30 \text{ W m}^{-2} \text{ h}^{-1}$ . Remarkably, surface-layer feedbacks are of negligible importance in a fully coupled system.

Analysis of the boundary-layer feedbacks hints the existence of two regimes in this feedback depending on atmospheric temperature, with a gradual transition region in between the two. In the low-temperature regime specific humidity variations induced by evapotranspiration and dry-air entrainment have a strong impact on the evapotranspiration. In the high-temperature regime the impact of humidity variations is less pronounced and the effects of boundary-layer feedbacks are mostly determined by temperature variations.

# 1. Introduction

The exchange of water between the land surface and the atmosphere is an essential component of the hydrologic cycle. Previous studies have shown that this exchange, evapotranspiration, is closely coupled to the atmosphere (e.g. Jacobs and De Bruin 1992; Betts et al. 1996; Koster et al. 2004). To be able to make credible predictions about the water balance of the earth in future climates, it is therefore fundamental to understand the driving mechanisms behind evapotranspiration and the link between the land surface and the atmospheric boundary-layer (ABL).

Evapotranspiration and land-atmosphere interactions have been the subject of many studies. These studies cover a large spectrum of spatial and temporal scales and range from conceptual studies to realistic 3D modeling. Relevant examples of large-scale studies using complex models are Betts et al. (1996), who discussed the memory of soil moisture and its impact on precipitation over a longer period, or Koster et al. (2004) who used an ensemble of GCMs to investigate the response of precipitation to soil moisture change by locating the regions with the strongest land-atmosphere coupling.

Then there are studies discussing land-atmosphere coupling on a local scale. Studies as De Bruin (1983) and McNaughton and Spriggs (1986) were the first to study the land surface, ABL and free atmosphere as a coupled system. Their finding that the ABL dynamics have an important influence on the surface evaporation formed the basis for more advanced studies. These are, for instance, Brubaker and Entekhabi (1995, 1996) and Margulis and Entekhabi (2001), who made mathematical frameworks to quantify feedbacks in the coupled land-atmosphere system. Furthermore, Ek and Holtslag (2004) quantified the

link between soil moisture, surface evapotranspiration and boundary-layer clouds. Recent studies discussing evapotranspiration from an atmospheric perspective are Santanello et al. (2007), who analyzed the existence of evaporation regimes as a function of soil moisture and atmospheric stability and Raupach (2000); van Heerwaarden et al. (2009), who investigated the impact of atmospheric temperature and moisture on surface exchange and the regulation of the surface energy balance by feedbacks.

What most of these studies have in common is that they investigate the response of the integrated set of all feedbacks mechanisms to variations in the properties of either the land surface or the atmosphere. To our knowledge, only the studies of Brubaker and Entekhabi (1996) and Margulis and Entekhabi (2001) have provided methods to quantify the influence of individual forcings and feedbacks in the coupled land-atmosphere system on evapotranspiration. Our study focuses on evapotranspiration on the diurnal time scale and is therefore complementary to the work of Brubaker and Entekhabi (1996). Their study aims at understanding the longer time scales involved in the heat and moisture budget, which can for instance be seen in their assumption of constant ABL height. In turn, we are mostly interested in time scales of one day and shorter and focus particularly on the dynamics of the ABL. The study of Margulis and Entekhabi (2001) covers a theoretical overview of the feedback pathways that exist in the land-atmosphere system on a diurnal time scale using an example based on the FIFE data (Sellers et al. 1992) and shows in a conceptual way how studying evapotranspiration using offline models can be misleading.

In this paper, we describe a method for quantifying forcings and feedbacks during daytime convective conditions and apply it to two real data cases. In comparison to Margulis and Entekhabi (2001) our method is designed to quantify forcings and feedbacks directly from

measurement or model data and is therefore complementary to their method.

The evapotranspiration is dependent on both the properties of the atmospheric boundary-layer and the land surface. The temperature and humidity of the atmosphere control the maximum amount of water that the atmosphere can take up, which is the potential evapotranspiration. The land surface properties, such as the vegetation characteristics and the soil texture and its moisture content, determine the supply of water, thus to which degree the evapotranspiration rate reaches the potential. In the coupled land-atmosphere system, all variables are connected through a set of feedback mechanisms (Brubaker and Entekhabi 1995; van Heerwaarden et al. 2009). For instance, an increase in soil moisture results in a larger evapotranspiration rate, which in turn has a positive effect on the atmospheric moisture content and a negative effect on the temperature as less energy is available for the sensible heat flux. In Section 2a we give a comprehensive description of the coupled land-atmosphere system, in which we define what we consider the forcings and the feedbacks that act on surface evapotranspiration.

The Penman-Monteith equation (Monteith 1965) provides a way to quantify surface evapotranspiration taking into account the capacity of the atmosphere to take up water, as well as the ability of the land surface to provide it. For this reason, it is the most widely used parameterization for evapotranspiration in atmospheric and hydrologic models. In this paper we show that by differentiating the Penman-Monteith equation with respect to time, we obtain a budget equation for evapotranspiration. This can be rewritten in a form that provides separate terms for all forcings and feedbacks that act on the evapotranspiration if it is combined with the mixed-layer equations (Lilly 1968; Tennekes 1973) that describe the most essential dynamics of the daytime ABL. In Section 2b we explain this budget equation

in detail.

Then, we demonstrate how are method can be used to analyze data to be able to identify the driving forces behind the daily cycle of evapotranspiration. Here, we use data of two contrasting locations. The two selected cases are 25 September 2003 at Cabauw, The Netherlands (Casso-Torralba et al. 2008) and 22 June 2006 at Niamey, Niger, measured during the AMMA campaign (Redelsperger et al. 2006). The first case is a typical mid-latitudes case, where evapotranspiration is energy-limited. This case is characterized by relatively cold temperatures, a moist and fully grass-covered land surface and only little advection. The second case corresponds to semi-arid conditions, where evapotranspiration is limited by the amount of available water. This case is a hot pre-monsoon day over a sparsely vegetated savanna, subjected to strong heat and moisture advection in the morning and a fast drying land surface throughout the day.

We reproduce the two days using a coupled land-atmosphere model. First, in Section 3 we discuss the model and the modeling experiment in detail and describe the data we use for the model evaluation. Second, in Section 4a we evaluate the model output against observations. In the subsequent analysis in Section 4b we apply our budget equation to the model result and do a thorough evaluation of all the terms in the budget equation. Per location we demonstrate how our method can be used to find out the importance of the forcings compared to the feedbacks in determining to which extent the evaporation is locally regulated. In this analysis, we compare the forcings, boundary-layer and land surface feedbacks in detail.

## 2. Evapotranspiration analysis framework

### *a. Overview of the coupled land-atmosphere system*

In this section we explain the elements of the coupled land-atmosphere system that are relevant for the daily evolution of evapotranspiration. Figure 1 shows all the variables that are contained in this system and which will later appear in the budget equation that we present in Section 2b.

The system essentially consists of three components. First, there is the land surface, which provides water and heat to the atmosphere through the surface evapotranspiration  $LE$  and the sensible heat flux  $H$ . The energy that is available for these two processes is the net radiation  $Q_*$ , which is the sum of incoming  $S_{in}$  and outgoing  $S_{out}$  short wave radiation and incoming  $L_{in}$  and outgoing  $L_{out}$  long wave radiation, minus the energy that enters the soil through the ground heat flux  $G$ . Land surface properties, such as the vegetation type and cover or soil moisture, are accounted for in the surface resistance  $r_s$ , whereas the turbulent characteristics of the near-surface atmosphere, which determine how efficient water is taken up, are accounted for in the aerodynamic resistance  $r_a$ .

Second, there is the convective atmospheric boundary-layer (ABL) that has a well-mixed profile for potential temperature  $\theta$  and specific humidity  $q$ . In this layer, the moisture that enters the ABL through the surface heat fluxes and the entrainment heat fluxes is vertically mixed by the convection. Large-scale temperature  $adv_\theta$  and moisture  $adv_q$  advection act on the thermodynamic state of the ABL, which subsequently feeds back on the surface evapotranspiration.

Third and last, there is the free atmosphere. Its potential temperature and specific



humidity minus the values in the ABL define the jumps of potential temperature  $\Delta\theta$  and specific humidity  $\Delta q$ . These jumps are strongly related to the vertical profiles of temperature and humidity in the free troposphere (see Equations A9 and A10). The first determines in a large extent the ABL growth, thus the evolution of the ABL height  $h$ , whereas the latter determines the amount of dry air that can be entrained during growth of the ABL.

In this study, we strictly separate forcings and feedbacks. As forcings we consider all processes that influence surface evapotranspiration, but which are not or only very weakly influenced by the state of the coupled land-atmosphere system on the time scale of one day. Therefore, these processes do not respond to the surface evapotranspiration, thus we assume them to be external forcings. As feedbacks on surface evapotranspiration, we consider the processes that react on the surface evapotranspiration and that, because of this reaction, have an influence on the evapotranspiration itself. Because these processes locally regulate the evapotranspiration, we call them feedbacks. In the next section we discuss the complete set of forcings and feedbacks in the system.

*b. Budget equation for surface evapotranspiration*

Now, we introduce the mathematical expression that describes the time evolution of evapotranspiration  $LE$  as a function of all forcings and feedbacks in the coupled land-atmosphere system sketched in Figure 1. This equation is acquired by combining a time derivative of the Penman-Monteith equation with the mixed-layer equations for the ABL (see Appendix A for a full derivation). Equation 1 shows the tendency of evapotranspiration ordered in forcings and feedbacks.

$$\begin{aligned}
\frac{dLE}{dt} &= \overbrace{c_0 \frac{dq_{sat}}{dT} \left\{ (1 - \alpha) \frac{dS_{in}}{dt} + \frac{dL_{in}}{dt} \right\}}^{\text{surface radiation forcings}} \\
&+ \overbrace{c_0 \left( H \frac{d^2 q_{sat}}{dT^2} + \frac{\rho c_p}{r_a} \frac{dq_{sat}}{dT} \right) \left\{ adv_\theta \right\} - c_0 \frac{\rho c_p}{r_a} \left\{ adv_q \right\}}^{\text{boundary-layer forcings}} \\
&+ \overbrace{c_0 \left( H \frac{d^2 q_{sat}}{dT^2} + \frac{\rho c_p}{r_a} \frac{dq_{sat}}{dT} \right) \left\{ \frac{H}{\rho c_p h} + \frac{w_e \Delta \theta}{h} \right\} - c_0 \frac{\rho c_p}{r_a} \left\{ \frac{LE}{\rho L_v h} + \frac{w_e \Delta q}{h} \right\}}^{\text{boundary-layer feedbacks}} \\
&- \overbrace{c_0 \left( \frac{\rho c_p}{r_a^2} (q_{sat} - q) - LE \frac{c_p}{L_v} \frac{r_s}{r_a^2} \right) \frac{dr_a}{dt}}^{\text{surface-layer feedback}} \\
&- \overbrace{c_0 \frac{dq_{sat}}{dT} \frac{dL_{out}}{dt} - c_0 \frac{dq_{sat}}{dT} \frac{dG}{dt} - c_0 LE \frac{c_p}{L_v} \frac{1}{r_a} \frac{dr_s}{dt}}^{\text{land surface feedbacks}} \\
c_0 &= \frac{1}{\frac{dq_{sat}}{dT} + \frac{c_p}{L_v} \left( 1 + \frac{r_s}{r_a} \right)} \tag{2}
\end{aligned}$$

with  $\frac{dq_{sat}}{dT}$  as change of saturated specific humidity with respect to temperature,  $c_p$  as the heat capacity of air at constant pressure,  $L_v$  the latent heat of vaporization,  $\rho$  the density of the atmosphere,  $w_e$  the entrainment velocity and  $\alpha$  the albedo of the land surface.

Each of the terms on the right hand side shows the contribution of a separate process to the time evolution of evapotranspiration. The terms can be interpreted as a sensitivity of evapotranspiration to a change in a variable  $\left(\frac{\partial LE}{\partial var}\right)$  multiplied with the tendency of that specific variable  $\left(\frac{dvar}{dt}\right)$ , although in the case of potential temperature and specific humidity, the tendency has been replaced by the mixed-layer equations (see Appendix A). The five lines, in which the terms are ordered in their respective category, represent the following:

- i. *Surface radiation forcings.* This forcing represents the effects of variations in the incoming radiation. The first term represents the net shortwave radiation, since the

outgoing shortwave is defined as the albedo  $\alpha$  multiplied with  $S_{in}$ , whereas the second term represents the incoming long wave radiation. Both are considered as external forcings. The net shortwave radiation represents the incoming solar energy, and since we do not take into account clouds here, it is therefore independent of the properties of the coupled land-atmosphere system. Although the incoming long wave radiation is function of the atmospheric temperature, it is rather insensitive to fluctuations in the ABL temperature on the time scale of one day, and is therefore assumed to be an external forcing. Both terms are positively related to the evapotranspiration tendency, for the reason that more available energy allows for more evapotranspiration.

- ii. *Boundary-layer forcings.* This forcing represents the large-scale processes that influence either the potential temperature or the specific humidity of the mixed-layer. In this study, where we do not consider clouds or radiation divergence in the atmosphere, this is only the large-scale advection. The first term describes the potential temperature advection. The second term represents the consequences of large-scale moisture advection. The boundary-layer forcings and feedbacks, shown in the next paragraph, enhance evapotranspiration if they warm or dry the ABL and reduce evapotranspiration if they cool or moisten the ABL.
- iii. *Boundary-layer feedbacks.* The first term of this forcing represents the effects of the surface (first term in bracket) and entrainment (second term in bracket) sensible heat flux on the potential temperature. The second term of this forcing describes the impact of evapotranspiration (first term in bracket) and dry-air entrainment (second term in bracket) on the specific humidity.

- iv. *Surface-layer feedbacks.* This term represents the impact of changes in the atmospheric resistance. If the atmosphere becomes more unstable or if the surface wind speed increases, then the atmospheric resistance decreases and evapotranspiration rises.
- v. *Land surface feedbacks.* This last term shows the effects of the three processes of which the land surface feedbacks consist. The first term represents the outgoing long wave radiation, which is a function of the surface temperature. The second term describes the ground heat flux, which is the part of the incoming radiation that enters the ground and is therefore not available for evapotranspiration. The third term accounts for variations in the surface resistance, which are induced by the response of the vegetation to changes in radiation or soil moisture or by the drying of the soil in the case of bare soil evaporation. An increase in outgoing long wave radiation results in a reduction of the evapotranspiration, because it reduces the net radiation. Similarly, a rise in the ground heat flux results in a decrease of evapotranspiration, as this reduces the available net radiation. An increase in surface resistance results in a fall in evapotranspiration as the land surface is less efficient in making water available for evapotranspiration.

### 3. Methods

#### *a. Model*

Here, we define the experiment to which we apply our framework. We use an extended version of the simple coupled land-atmosphere model which is described in van Heerwaarden et al. (2009). This model is inspired on the early studies of De Bruin (1983) and Mc-

Naughton and Spriggs (1986) and has proven to be successful in reproducing the essential land-atmosphere feedbacks accurately. The atmospheric part of the model is described in Appendix A by equations A5 to A10, and is based on Lilly (1968) and Tennekes (1973). We have extended these models by including a simple radiation model, dynamical models for the aerodynamic and surface resistance and a soil model.

In the simple radiation model the incoming short wave radiation is a function of the time, day, latitude and longitude and the incoming long wave radiation a function of the mixed-layer temperature.

To calculate the atmospheric resistance we include stability corrections based on Monin-Obukhov similarity theory, using the integrated flux-gradient relationship as proposed by Paulson (1970). For this, we evaluate the gradient at the top of the surface-layer, assuming that this height is at 0.1 of the boundary-layer height that is calculated by the atmospheric model.

To mathematically describe the land surface and to be able to model partially vegetated surfaces, we have introduced a force-restore soil model. The surface energy balance and temperature equations are based on Duynkerke (1991), whereas the soil moisture equations are based on Noilhan and Planton (1989). We chose the soil temperature description of Duynkerke (1991) over that of Noilhan and Planton (1989) since this formulation yields more accurate ground heat fluxes for nearly fully vegetated surfaces as in Cabauw. Since, in contrast to van Heerwaarden et al. (2009), we have added a soil model, the ground heat flux is resolved and therefore no longer a fixed fraction of the net radiation.

The evapotranspiration calculated by the model is a sum of three components: transpiration from vegetation, evaporation from bare soil and evaporation from wet foliage. A

bulk surface resistance  $r_s$  is diagnosed from this sum and used in our budget equation for evapotranspiration. The computation of the transpiration from vegetation requires a canopy resistance, which we compute using the Jarvis-Stewart model (Jarvis 1976) (see Appendix B for a full description). We added a parametrization to take into account the impact of interception water and dew formation on evapotranspiration (Viterbo and Beljaars 1995).

*b. Numerical experiments*

1) CABAUW, THE NETHERLANDS: 25 SEPTEMBER 2003

For our first case, we have selected measurements from Cabauw, The Netherlands, observed during 25 September 2003 (Casso-Torralba et al. 2008). This was a cloudless day with negligible horizontal advection for heat and moisture. The early morning profile was characterized by a large and moist residual layer, which had a very strong inversion on top of it above which the atmosphere was relatively dry. In Appendix C we have included a list of all model parameters, initial conditions and boundary conditions for this study.

To evaluate our model results, we use tower measurements of temperature and dew point temperature taken at 140 m to calculate the mixed-layer temperature  $\theta$  and the mixed-layer specific humidity  $q$ . In addition, we compare surface measurements of incoming and outgoing short and long wave radiation with the radiation balance calculated by the model. Furthermore, we evaluate the calculated surface sensible  $H$  and latent  $LE$  heat flux against 10-min eddy correlation data, measured at 3 m above the land surface. The calculated atmospheric boundary-layer height  $h$  is evaluated against low-mode wind profiler measurements.

## 2) NIAMEY, NIGER: 22 JUNE 2006

For the second case, we have selected 22 June 2006 measured during the AMMA campaign (Redelsperger et al. 2006). This was a nearly cloudless day in the early stage of the monsoon. Deep convection with heavy rainfall occurred during the previous night, which provided water to the soil. A large part of this water was already removed via run-off, drainage or evaporation during the night. There is a large diurnal cycle of temperature combined with a strong drying of the soil throughout the day. In addition, both the moisture and the temperature balance are significantly affected by advection of relatively moist and cold air, which ceases in the afternoon.

To validate the model, we use surface measurements of the ARM mobile facility (Miller and Slingo 2007) that measured the surface energy and radiation balance at the location. The mixed-layer potential temperature  $\theta$  and specific humidity  $q$  are validated by comparing them to four radiosoundings taken at intervals of three hours. From these radiosoundings, the boundary-layer height  $h$  is constructed by picking the lowest height at which the virtual potential temperature at that specific height is 0.25 K higher than the mean from the land surface to that height. The mixed-layer potential temperature and humidity are acquired by averaging the radiosounding from the land surface to the boundary-layer height. The turbulent fluxes of temperature and moisture that represent the sensible  $H$  and latent  $LE$  heat flux are compared with eddy correlation measurements taken at the airport of Niamey, where the vegetated part of the land surface is covered with grass. Initial soil temperatures are close to those measured at the nearby station of Wankama. Large scale advection tendencies are estimated from the ECMWF re-analysis data for the AMMA observational

campaign.

## 4. Results

### *a. Model validation*

#### 1) CABAUW, THE NETHERLANDS

We start our analysis by verifying the capability of the model to reproduce the measurements of the selected case of 25 September 2003. First, we compare the measured and modeled radiation balance, which confirms a close match between the model and the observations (not shown). Second, we validate the model against the measured potential temperature, specific humidity, boundary-layer height and surface heat fluxes (see Figure 2).

Here, we find a satisfactory agreement between the measured and modeled boundary-layer height, potential temperature and specific humidity, which is a confirmation that our conceptual model captures the most relevant dynamics of the coupled land-atmosphere system. The data of the boundary-layer height shows significant fluctuations in the afternoon, which could be related to the measurement error in this data which could reach 40 per cent (Steenefeld et al. 2007). Nevertheless, the fact that our model reproduces the time evolution of the specific humidity well is an indication that the complex interplay of surface and entrainment fluxes is correctly represented by the model. Note that between 7h30 and 8h10 UTC the modeled potential temperature and specific humidity deviate strongly from the measurements. In the early morning phase, the ABL is not yet well-mixed, whereas within our model setup, we assume it to be. This causes a deviation from the observations that



quickly disappears after 8 h UTC, when the ABL becomes well-mixed.

The modeled surface heat fluxes show larger differences with the observed data than the temperature and humidity, although they approximately capture the values and tendencies. Since closing the surface energy balance is notoriously difficult using eddy covariance data (Brotzge and Crawford 2003) and the tower has a different footprint than the surface flux measurements, we assume that the correct reproduction of the boundary-layer properties confirms that we model the appropriate fluxes.

## 2) NIAMEY, NIGER

Also for the second case, the model compares well with the measurements. There is a close match between the measured and modeled radiation at the surface, which confirms that we prescribe the right available energy to the model (not shown). In addition, the modeled surface heat fluxes and the height, temperature and humidity of the mixed-layer match well with the observations (see Figure 3). This is confirmed by a comparison of the mixed-layer profiles with radiosoundings taken at 3-hour intervals during this day, shown in Figure 4. The figure proves the quality of the mixed-layer model in convective conditions. The potential temperature and the specific humidity are described well over the whole mixed-layer depth by a single value. Only in the profile of 17h40 UTC, a limited gradient is observed in the top of the mixed-layer for both temperature and moisture. At this time the virtual heat flux at the surface is barely positive anymore (see Figure 3) and the mixing is therefore less intense.

The surface evapotranspiration measurements show a good match with the modeled evapotranspiration, but the modeled values are slightly higher than the observations. Since

the curve describing the modeled evapotranspiration follows the complex tendency of the observations well, we can assume that both the processes at the land surface and in the atmosphere are adequately reproduced by the model. The fact that large part of the rain water already left the system during the night, explains the fast decline of the evapotranspiration during the day, as the reservoir is quickly depleted. The sensible heat flux is, similar to the evapotranspiration, larger in the model results than in the observations. Under the conditions of Niamey, a non-closure of the surface energy balance up to 20 percent of the net radiation is very common (Ramier et al. 2009). In our case, this would indicate a loss of approximately  $100 \text{ W m}^{-2}$ , which is more than the difference between the modeled and the observed surface fluxes. Since we are able to reproduce the radiosoundings, we assume that the modeled surface heat fluxes are representative for our case.

To conclude, the land-atmosphere model is able to reproduce the most important boundary-layer and surface flux characteristics of the two selected cases, therefore validating the application of the model output data as input for our evapotranspiration analysis framework.

*b. Analysis of the daily cycle of evapotranspiration*

1) OVERVIEW OF FORCINGS AND FEEDBACKS

We start the analysis of evapotranspiration by showing in Figure 5 an overview of the total tendency of evapotranspiration and the separate contribution of the five categories of forcings and feedbacks defined in Equation 1.

According to the figure, there are strong similarities as well as differences between the two cases. In both cases, the surface radiation forcing is the main external driver of the

system. It contributes positively in the morning when the sun rises fast, adding more than  $30 \text{ W m}^{-2} \text{ h}^{-1}$  to the evapotranspiration. Then, at 11h40 UTC at Cabauw and at 12 h UTC at Niamey it crosses the zero-line, marking the position of the sun closest to the zenith, and during the remainder of the day the contribution becomes more negative as the angle between the sun and the zenith increases again. In Cabauw, the surface radiation forcings decrease linearly over the the majority of the day, whereas in Niamey, the slope of the line representing the forcing is less negative in the afternoon than in the morning, thus radiation is less effective in influencing the surface evapotranspiration later during the day. It is also found that the impact of heat and moisture advection on evapotranspiration is minimal in Niamey. In Section 4, we will explain these findings after an in-depth analysis of the forcings.

Despite the similarities in the surface radiation forcings, there is a large difference in the time evolution of the evapotranspiration tendency of the two cases. A first explanation is that in Cabauw the three feedbacks (see Figure 5, panel c and d) add up to a positive tendency during the majority of the day, whereas in Niamey they add up to negative values most of the day. The differences in the feedbacks can also be found in the plot showing the forcings (see Figure 5, panel a and b). In the case of Cabauw, the total tendency is larger than the tendency induced by the forcings during the period from 9 h UTC to 14 h UTC, which implies that the feedbacks enhance evapotranspiration. The case of Niamey shows the opposite. Here, the total tendency is less than than the tendency induced by the forcings alone until 14 h UTC. Therefore, the impact of the feedbacks must be negative most of the day.

The cause for the large difference between the cases can be found in the land surface feedbacks. In the case of Cabauw, the land surface feedback has only a modest negative

impact in the morning with a minimum at  $-17 \text{ W m}^{-2} \text{ h}^{-1}$  at 8 h UTC. Thereafter, its value quickly rises and after 12 h UTC its contribution is negligible. In Niamey we find a much larger negative impact, reaching  $-35 \text{ W m}^{-2} \text{ h}^{-1}$  just after 10 h UTC and remaining significantly negative until 16 h UTC. In Section 2 we elaborate the land surface feedbacks in the two cases and discuss the differences in the driving mechanisms between the two cases, to be able to explain this large difference.

In contrast to the land surface feedbacks, the contribution of the boundary-layer feedbacks is comparable between the two cases. Both have a rising contribution in the morning, with a peak near 10 h UTC of  $20 \text{ W m}^{-2} \text{ h}^{-1}$  and are thereafter gradually reducing towards zero. The similarity between the two cases is striking, as there is a large difference in the partitioning of the surface fluxes, and in the related time evolution of the ABL properties (see Figures 2 and 3). In Section 3 we discuss the boundary-layer feedbacks in detail.

In both cases, the surface-layer feedback is of low importance throughout the majority of the day. Only in the early morning at the start of convection and in the evening transitions when convection stops, its contribution is large. The weak influence of surface-layer feedbacks is because the relative changes in the aerodynamic resistance are small, because the resistance is strongly buffered in the coupled system. This is caused by the inverse relationship between the drag coefficient and the wind, from which  $r_a$  is computed by  $r_a = (C_D U)^{-1}$ . This relation implies that if wind speed increases, the surface-layer becomes less unstable, thus  $C_D$  decreases and vice versa. The irrelevance of the surface-layer feedback confirms the findings of McNaughton and Spriggs (1986), who found that in coupled models, the evapotranspiration is insensitive to the aerodynamic resistance.

To summarize, we have three open questions now, which we will answer by analyzing the

boundary-layer feedbacks, land surface feedbacks and forcings in detail using our method. First, we analyze what drives the land surfaces feedbacks in both location. Second, we explain why the boundary-layer feedbacks are so similar in both cases, despite the striking differences between the two cases. Third, we explain why the radiation forcing is less efficient in the afternoon in Niamey, while it retains its strength in Cabauw and why the impact of advection is so small in Niamey.

## 2) LAND SURFACE FEEDBACKS

In Figure 6 we show the land surface feedbacks, decomposed into the three terms shown in Equation 1, which are related to the outgoing long wave radiation, the ground heat flux and the surface resistance. It is the evolution of the surface resistance feedback that makes the large difference between the two cases, having only little dynamics in Cabauw, in contrast to a large diurnal cycle over Niamey. In Cabauw, the contribution is slightly negative throughout the whole day with a minimum of  $-5 \text{ W m}^{-2} \text{ h}^{-1}$  at 8 h UTC, then rising slightly towards  $0 \text{ W m}^{-2} \text{ h}^{-1}$  near 11 h UTC, and thereafter gradually falling until  $-10 \text{ W m}^{-2} \text{ h}^{-1}$  in the evening transition when convection stops. In the morning there is dew on the leaves which makes evaporation at the potential rate possible for a limited fraction of the vegetation. The dew water reservoir depletes quickly and the surface resistance consequently rises, thus explaining the modest peak at 8 h UTC. The gradually increasing negative impact in the afternoon is explained by the response of the plants to the fall in shortwave radiation. The time evolution of the surface variables of Cabauw (see Figure 7) demonstrates the modest temperature range, and the limited increase of the surface resistance in the morning.

In Niamey, the surface resistance feedback falls to  $-28 \text{ W m}^{-2} \text{ h}^{-1}$  from the moment that convection starts until 10h30 UTC. Afterwards, the impact of the feedbacks reduces considerably, reaching a maximum of  $-8 \text{ W m}^{-2} \text{ h}^{-1}$  at 15h20 UTC, but falls thereafter again. Over Niamey, the majority of the evapotranspiration is bare soil evaporation. Since there has been precipitation during the night, the day starts with a moist soil. First, the evapotranspiration is rising (see Figure 3), thereby depleting the soil moisture at an increasing rate and progressively increasing the surface resistance. Note that despite the fast increase of the resistance, the evapotranspiration is initially still rising, because the forcings and boundary-layer feedback compensate for it (see Figure 5). This phase is pointed out by Brubaker and Entekhabi (1995), who show that anomalies in soil moisture are reinforced by a rise in surface temperature. This rise can be found in Figure 7 that shows the time evolution of surface and soil temperature.

After reaching the evapotranspiration peak just before 10 h UTC, the water in the top soil layer gets depleted. Although the resistance increases at a high pace (see Figure 7), the increase of large resistances to even larger resistances only has a limited effect on the evapotranspiration. Therefore, the contribution of the surface resistance to the tendency of evapotranspiration becomes less negative in time.

The contributions of the long wave radiation and the ground heat flux to the land surface feedbacks are similar for the two cases, slightly negative in the morning ( $-5 \text{ W m}^{-2} \text{ h}^{-1}$  for Cabauw and  $-10 \text{ W m}^{-2} \text{ h}^{-1}$  for Niamey) and almost linearly increasing throughout the day and is changing to positive sign around noon. Both feedbacks are inversely related to the incoming radiation. If the incoming radiation rises, the surface temperature rises. This means that more energy enters the soil through the ground heat flux and that more of the

incoming radiation leaves the surface via the outgoing long wave radiation. Consequently, there is a negative impact on the evapotranspiration. Shortly after the moment that the sun reaches its smallest angle to the zenith, the surface temperature starts decreasing, and both contributions become positive, because the decrease in soil heat flux and outgoing long wave radiation makes more energy available for evapotranspiration. The amplitude of these two contributions is larger in Niamey compared to Cabauw, because the larger diurnal range of surface temperatures.

### 3) BOUNDARY-LAYER FEEDBACKS

Here, we compare in detail the boundary-layer feedbacks of the two cases. To be able to quantify the relevance of each individual boundary-layer process, we calculate the four components of the boundary-layer feedbacks shown in Equation 1 (see Figure 8).

Although we concluded in the previous analyses that there is a similar total contribution of the boundary-layer feedbacks between the two cases, there is a considerable difference in the magnitude of the four terms that add up to the total. In Cabauw the boundary-layer feedbacks are just as much influenced by the temperature related processes as the moisture related processes. In the morning when the boundary-layer is warming fast, between 9 and 10 h UTC, the increase of the temperature by surface heating has a positive contribution to the evapotranspiration close to  $10 \text{ W m}^{-2} \text{ h}^{-1}$ . This positive enhancement is more than compensated by the decrease of the evapotranspiration caused by the moistening of the air which is close to  $-10 \text{ W m}^{-2} \text{ h}^{-1}$  until 10 h UTC. Later during the day, the effects of the surface heat fluxes become less, due to boundary-layer growth: now the surface fluxes enter

a larger reservoir, the fully developed ABL, and therefore require more time to modify the atmospheric temperature or specific humidity.

The effect of entrainment is well-pronounced. Especially the effect of dry-air entrainment, at 10h40 UTC, has a strong positive contribution to the surface evapotranspiration of  $15 \text{ W m}^{-2} \text{ h}^{-1}$ . At this time the boundary-layer grows the fastest and is still relatively moist (see Figure 2). The quick drop of specific humidity (from  $5.5$  to  $4.6 \text{ g kg}^{-1}$ ) occurring then has a strong influence on the moisture deficit and thus on the evapotranspiration. The effect of temperature entrainment contributes also significantly to the surface evapotranspiration. The distinct peak, which we find in moisture is however absent, because temperature entrainment fluctuates less throughout the day than moisture entrainment and is, except for the early morning, in magnitude smaller than the surface sensible heat flux.

In Niamey, the boundary-layer feedbacks are mostly controlled by temperature. The surface warming feedback contributes up to  $13 \text{ W m}^{-2} \text{ h}^{-1}$  to the time evolution, whereas the other three feedbacks have only a limited influence ranging from  $-2 \text{ W m}^{-2} \text{ h}^{-1}$  for the surface evapotranspiration until approximately  $3 \text{ W m}^{-2} \text{ h}^{-1}$  for both entrainment fluxes.

The difference between the boundary-layer feedbacks in Cabauw and those in Niamey have two explanations. First, the evapotranspiration flux is smaller in Niamey. Therefore, the opportunity for evapotranspiration to moisten the atmosphere to influence evapotranspiration significantly is limited. Nevertheless, there is a large dry-air entrainment flux in Niamey, thus we need another explanation for the low sensitivity of the evapotranspiration to that. The answer is in the nonlinear relationship between saturated specific humidity and temperature, described by the Clausius-Clapeyron relationship, plotted in Figure 9. If the temperature is relatively low, such as in Cabauw, then variations in the moisture deficit



$q_{sat} - q$  are just as dependent on variations in temperature as on variations in moisture. In conditions of higher temperatures, however, the saturated specific humidity is much more sensitive to variations in the temperature than at low temperatures. Therefore, variations in the moisture deficit are mainly caused by variations in temperature. To illustrate this: in Cabauw,  $q_{sat}$  changes from 10.0 to 12.3 g kg<sup>-1</sup> from 10 to 15 h UTC (see Figure 9), where  $q$  changes from 5.6 to 4.9. In Niamey, however,  $q_{sat}$  increases from 27.4 to 38.0 g kg<sup>-1</sup> between 10 and 15 h UTC (see Figure 9), whereas  $q$  only decreases from 13.5 to 10.9 g kg<sup>-1</sup>. From this analysis, we can conclude that due to the nonlinear relation between temperature and saturated humidity dry-air entrainment is particularly significant at lower temperatures. These observed cases confirm thus the theoretical experiments of van Heerwaarden et al. (2009), who showed that the impact of dry-air entrainment becomes less at higher temperatures. Our finding also extend previous studies to the effect of dry-air entrainment in the Sahel region (Lothon et al. 2007; Canut et al. 2010), by showing that dry-air only has a minimal impact on the surface heat fluxes, despite its large impact on the specific humidity and thus on cloud formation and convection. In between these two regimes, there is a gradual transition from one regime into the other. This becomes clear in the results of Margulis and Entekhabi (2001), who analyzed a case in which the temperature is significantly higher than in Cabauw, but less than in Niamey, while the Bowen ration resembles that of the Cabauw case. In their results, the sensitivity of evapotranspiration to the free atmospheric humidity is less than in our Cabauw case, and less than the impact of temperature on evaporation, but it is clearly larger than the impact of free atmospheric humidity in the case of Niamey.

To come back to the question why the boundary-layer feedbacks are so similar between the two cases: this is coincidental as an in-depth analysis shows that there are significant

differences between the four contributions of the boundary-layer feedbacks.

#### 4) FORCINGS

In Figure 10 we give an overview of the forcings of the coupled land-atmosphere system in the two cases. This figure completes the overview of all the terms that were shown in Equation 1. In both cases the total forcings are mainly depending on the contribution of incoming shortwave radiation, since both curves in the figure nearly overlap. In the first subsection of Section 4b we found that the impact of the forcings reduces in the afternoon in Niamey, while this is not the case in Cabauw. The explanation for this is related to difference in land surface feedbacks discussed in Section 2. Due to the drying of the soil and the subsequent increase in the surface resistance, the evaporation is strongly limited by the land surface conditions. The response of the evapotranspiration to falling radiation is therefore limited, since at this time the case is fully water-limited and radiation is no longer a limiting factor for evapotranspiration.

Based on this figure, we can argue that our assumption that the incoming long wave radiation is an external forcing is correct. In both situations the daily dynamics of the atmospheric temperature barely influence the impact of the incoming long wave radiation.

There is one extra feature in the forcings of Niamey, which is the large-scale advection of moist and cold air. This gradually decreasing advection has a slight negative impact on the evapotranspiration. Initially, the temperature advection has an impact of  $-3 \text{ W m}^{-2} \text{ h}^{-1}$ , which gradually increases to  $0 \text{ W m}^{-2} \text{ h}^{-1}$ . The moisture advection does not exert any influence at all. The explanation is similar to that of the insensitivity of evapotranspiration

to dry-air entrainment at high temperatures: the moisture deficit is largely determined by temperature variations and only little by variations in specific humidity.

## 5. Conclusion

A method to analyze the daily cycle of surface evapotranspiration has been developed. It reveals novel insights in the driving mechanisms behind surface evapotranspiration during the day. The method shows clearly that surface evapotranspiration is a complex process that can only be understood by considering the land surface and the atmosphere as an interactive system. It quantifies separately variations in the surface evapotranspiration driven by direct forcings, such as radiation, as well as those driven by feedbacks that exist between evapotranspiration and the land surface, the surface-layer and the atmospheric boundary-layer (ABL).

We modeled and validated with data two contrasting observed cases, 25 September 2003 at Cabauw, The Netherlands and 22 June 2006, Niamey, Niger. The first case is a characteristic example of a case in which evapotranspiration is energy-limited, whereas the second is a typical water-limited case. Subsequently, we apply our method to the model output. This reveals insights in the mechanisms that drive evapotranspiration at these locations.

We find that forcings and feedbacks are of equal importance in the control of surface evapotranspiration. The local conditions determine how much the feedbacks enhance or suppress the forcings. In Cabauw, the feedbacks enhance evapotranspiration, because their sum is positive over the majority of the day. In Niamey the opposite is true. Here, the sum of the feedbacks is mostly negative, which indicates that evapotranspiration is suppressed

by the land-atmosphere system. In both cases the boundary-layer feedbacks, the effects of changes in the temperature and moisture content of the ABL, have an enhancing effect on evapotranspiration. In the case of Niamey, this effect is offset by the strong negative influence of the land surface feedbacks, induced by the drying of the soil.

Despite the similarity in the sign and magnitude of the boundary-layer feedbacks in both cases, there is a large difference in the processes that drive them. In the case of Cabauw, the variations of moisture and temperature in the atmosphere play an equally important role, and dry-air entrainment has the largest contribution to the boundary-layer feedbacks. In Niamey, however, the effect of temperature fluctuations dominates the feedbacks and moisture fluctuations become irrelevant. In general, it should be true that over cold areas in the world, both the atmospheric moisture and temperature regulate the boundary-layer feedbacks. If we move towards regions with high temperatures, we expect a gradual transition towards a regime where the boundary-layer feedbacks become temperature-controlled.

Although our method shows interesting features of the diurnal cycle of evapotranspiration, we would like to stress that our conclusions are only based on two cases that mainly served as examples of our new method. To acquire a solid understanding of the driving forces behind the daily cycle of evapotranspiration, future studies, which take into account longer time periods and more locations, are necessary. Such studies could enable us to identify for different areas in the world to which changes in the environment the evapotranspiration would be the most sensitive and how this sensitivity varies in space and time. This could for instance be done using output of weather and climate models. Before such studies can be undertaken, our model needs to be extended to cloudy boundary-layers.

### *Acknowledgments.*

The first author acknowledges Météo-France for supporting his research visit. This study was supported by a grant from the Netherlands Organization for Scientific Research (NWO TopTalent). The authors acknowledge the Royal Netherlands Meteorological Institute (KNMI) and Fred Bosveld for making available the Cabauw data.

## APPENDIX A

### **Derivation of evapotranspiration tendency equation**

In this appendix we derive the tendency equation for evapotranspiration from the Penman-Monteith equation and the mixed-layer equations that describe the daytime ABL.

$$LE = \frac{\frac{dq_{sat}}{dT} (Q_* - G) + \frac{\rho c_p}{r_a} (q_{sat} - q)}{\frac{dq_{sat}}{dT} + \frac{c_p}{L_v} \left(1 + \frac{r_s}{r_a}\right)} \quad (\text{A1})$$

The Penman-Monteith equation (equation A1) describes the actual evapotranspiration taking into account all processes that create a moisture gradient between the land surface and the atmosphere. These are the available energy, defined as the net radiation  $Q_*$  minus the soil heat flux  $G$ , and the moisture deficit of the air, which is the saturated specific humidity of the atmosphere  $q_{sat}$  minus its specific humidity  $q$ . The extent to which moisture can be

transported over this gradient is determined by the turbulence near the surface, described by the aerodynamic resistance  $r_a$  and the ability of the vegetation and soil to evaporate water, described by the surface resistance  $r_s$ . Note that the terms in the equation are in units of specific humidity rather than the more commonly used vapor pressure to facilitate the coupling with our atmospheric model.

If we differentiate this expression in time and group all the terms in the equation per tendency of each of the involved variables and finally replace  $Q_* - G - LE$  by  $H$ , we obtain equation A3.

$$c_0 = \frac{1}{\frac{dq_{sat}}{dT} + \frac{c_p}{L_v} \left(1 + \frac{r_s}{r_a}\right)} \quad (\text{A2})$$

$$\begin{aligned} \frac{\partial LE}{\partial t} &= c_0 \frac{dq_{sat}}{dT} \frac{dQ_*}{dt} & (\text{A3}) \\ &- c_0 \frac{dq_{sat}}{dT} \frac{dG}{dt} \\ &+ c_0 \left( H \frac{d^2 q_{sat}}{dT^2} + \frac{\rho c_p}{r_a} \frac{dq_{sat}}{dT} \right) \frac{dT}{dt} \\ &- c_0 \frac{\rho c_p}{r_a} \frac{dq}{dt} \\ &- c_0 \left( \frac{\rho c_p}{r_a^2} (q_{sat} - q) - LE \frac{c_p}{L_v} \frac{r_s}{r_a^2} \right) \frac{dr_a}{dt} \\ &- c_0 LE \frac{c_p}{L_v} \frac{1}{r_a} \frac{dr_s}{dt} \end{aligned}$$

With the previous equation, we have decomposed the evolution of evaporation in one term per involved variable. Nevertheless, the tendency of each variable is also the sum of a set of physical processes. We elaborate now some of the terms to improve the physical interpretation.

First, we split the net radiation tendency into the sum of the tendencies of the net short

wave and long wave radiation,

$$\frac{dQ_*}{dt} = (1 - \alpha) \frac{dS_{in}}{dt} + \frac{dL_{in}}{dt} - \frac{dL_{out}}{dt} \quad (\text{A4})$$

where  $\alpha$  is the albedo,  $S_{in}$  is the incoming short wave radiation at the surface,  $L_{in}$  is the incoming long wave radiation at the surface and  $L_{out}$  is the outgoing long wave radiation at the surface.

Second, we introduce the essential dynamics of the atmosphere into the temperature and moisture equation. Previous studies (Betts 1992; Santanello et al. 2009) show that the time evolution of the near-surface temperature and humidity is the effect of both external forcings such as advection and radiation divergence, as well as internal feedbacks such as the surface fluxes of heat and moisture and the entrainment fluxes of heat and moisture, which is the interaction between the turbulent boundary-layer and the free atmosphere above.

During daytime, the effects of the large-scale forcings and feedbacks are rapidly mixed throughout the atmospheric boundary-layer. Therefore, the layer can be considered as well-mixed and one value of the conserved variables specific humidity and potential temperature is representative for that layer. This yields the widely applied mixed-layer model (Lilly 1968; Tennekes 1973),

$$w_e = A_{\theta_v} \frac{\frac{H}{\rho c_p} + \theta \left( \frac{R_v}{R_d} - 1 \right) \frac{LE}{\rho L_v}}{\Delta \theta_v} \quad (\text{A5})$$

$$\frac{dh}{dt} = w_e + w_s \quad (\text{A6})$$

$$\frac{d\theta}{dt} = \frac{1}{h} \left( \frac{H}{\rho c_p} + w_e \Delta \theta \right) + adv_\theta \quad (\text{A7})$$

$$\frac{dq}{dt} = \frac{1}{h} \left( \frac{LE}{\rho L_v} + w_e \Delta q \right) + adv_q \quad (\text{A8})$$

$$\frac{d\Delta \theta}{dt} = \gamma_\theta \frac{dh}{dt} - \frac{d\theta}{dt} \quad (\text{A9})$$

$$\frac{d\Delta q}{dt} = \gamma_q \frac{dq}{dt} - \frac{dq}{dt} \quad (\text{A10})$$

with  $w_e$  as the entrainment velocity,  $A_{\theta_v}$  as the ratio between the entrainment virtual heat flux and the surface virtual heat flux,  $\rho$  as the density of air,  $c_p$  as the heat capacity of air at constant pressure,  $R_v$  as the gas constant of moist air,  $R_d$  as the gas constant of dry air,  $w_s$  as the large-scale vertical motion.

The most important assumptions that are enclosed in this model are:

- The ABL is well-mixed, therefore one value for the potential temperature and specific humidity is used for the whole layer (see sketch of vertical profiles in Figure 1).
- The boundary-layer growth (see Equation A6) is driven by the large-scale vertical velocity  $w_s$  and the surface virtual potential temperature flux (see Equation A5 where this value is written in terms of the heat fluxes). The entrainment parameter  $A_{\theta_v}$  relates the entrainment flux of virtual potential temperature to the surface flux. The entrainment zone is assumed to be of infinitesimal thickness (see sketch of vertical profiles in Figure 1).
- The prognostic equations for the jumps of potential temperature and specific humidity



between the ABL and the free atmosphere (see Equations A9 and A10) show that the jump is a competition of boundary-layer growth and the time evolution of the mixed-layer values of potential temperature (see Equation A7) and specific humidity (see Equation A8).

A complete description of all the physical assumptions behind the model can be found in Tennekes (1973).

Equation A7 and A8 are used to replace the temperature and moisture tendencies in Equation A3, thereby assuming that at the land surface the absolute temperature and the potential temperature are equal.

## APPENDIX B

### Detailed description of Jarvis-Stewart model

In our model the surface resistance  $r_s$  is modeled using a Jarvis-Stewart model with the following specifications:

$$r_s = \frac{r_{s,min}}{LAI} f_1(S_{in}) f_2(w) f_3(VPD) f_4(T) \quad (\text{B1})$$

with  $r_{s,min}$  as the minimum surface resistance,  $LAI$  as the leaf area index of the vegetated fraction,  $f_1$  as a correction function depending on incoming short wave radiation  $S_{in}$ ,  $f_2$  as a function depending on soil moisture  $w$ ,  $f_3$  as a function depending on vapor pressure deficit

$VPD$  and  $f_4$  as a function depending on temperature  $T$ .

The correction functions, where the first three are taken from the ECMWF IFS and the fourth from Noilhan and Planton (1989), are:

$$\frac{1}{f_1(S_{in})} = \min \left( 1, \frac{0.004S_{in} + 0.05}{0.81 (0.004S_{in} + 1)} \right) \quad (\text{B2})$$

$$\frac{1}{f_2(w)} = \frac{w - w_{wilt}}{w_{fc} - w_{wilt}} \quad (\text{B3})$$

$$\frac{1}{f_3(VPD)} = \exp(g_D VPD) \quad (\text{B4})$$

$$\frac{1}{f_4(T)} = 1.0 - 0.0016(298.0 - T)^2 \quad (\text{B5})$$

where  $w_{wilt}$  is the volumetric soil moisture at wilting point,  $w_{fc}$  is the volumetric soil moisture at field capacity and  $g_D$  is a correction factor for vapor pressure deficit.

## APPENDIX C

### Initial and boundary conditions coupled model

Table 1 and Table 2 show the initial and boundary conditions of the two cases.

## REFERENCES

- Betts, A. K., 1992: FIFE atmospheric boundary layer budget methods. *J. Geophys. Res.*, **97**, 18 525–18 531.
- Betts, A. K., J. H. Ball, A. C. M. Beljaars, M. J. Miller, and P. A. Viterbo, 1996: The land surface-atmosphere interaction: A review based on observational and global modeling perspectives. *J. Geophys. Res.*, **101**, 7209–7225.
- Brotzge, J. A. and K. C. Crawford, 2003: Examination of the surface energy budget: a comparison of eddy correlation and bowen ratio measurement systems. *J. Hydrometeor.*, **4**, 160–178, doi:10.1175/1525-7541(2003)4(160:EOTSEB)2.0.CO;2.
- Brubaker, K. L. and D. Entekhabi, 1995: An analytic approach to land-atmosphere interaction, 1, Model construct and equilibrium results. *Water Resour. Res.*, **31**, 619–632.
- Brubaker, K. L. and D. Entekhabi, 1996: Analysis of feedback mechanisms in land-atmosphere interaction. *Water Resour. Res.*, **32**, 1343–1357.
- Canut, G., M. Lothon, F. Saïd, and F. Lohou, 2010: Observations of entrainment at the interface between monsoon flow and the Saharan air layer. *Quart. J. Roy. Meteor. Soc.*, **136**, 34–46, doi:10.1002/qj.471.
- Casso-Torralba, P., J. Vilà-Guerau de Arellano, F. Bosveld, M. R. Soler, A. Vermeulen, C. Werner, and E. Moors, 2008: Diurnal and vertical variability of the sensible heat and

- carbon dioxide budgets in the atmospheric surface layer. *J. Geophys. Res.*, **113**, D12 119, doi:10.1029/2007JD009583.
- De Bruin, H. A. R., 1983: A model for the Priestley-Taylor parameter  $\alpha$ . *J. Applied Met.*, **32**, 572–578, doi:10.1175/1520-0450(1983)022<0572:AMFTPT>2.0.CO;2.
- Duykerke, P. G., 1991: Radiation fog: A comparison of model simulation with detailed observations. *Mon. Wea. Rev.*, **119** (2), 324–341.
- Ek, M. B. and A. A. M. Holtslag, 2004: Influence of soil moisture on boundary layer cloud development. *J. Hydrometeor.*, **5**, 86–99.
- Jacobs, C. J. M. and H. A. R. De Bruin, 1992: The sensitivity of regional transpiration to land-surface characteristics: significance of feedback. *J. Climate*, **5**, 683–698, doi:10.1175/1520-0442(1992)005<0683:TSORTT>2.0.CO;2.
- Jarvis, P. G., 1976: The interpretation of the variations in leaf water potential and stomatal conductance found in canopies in the field. *Philos. Trans. Roy. Soc. London*, **273B**, 593–610.
- Koster, R. D., et al., 2004: Regions of strong coupling between soil moisture and precipitation. *Science*, **305**, 1138–1140, doi:10.1126/science.1100217.
- Lilly, D. K., 1968: Models of cloud-topped mixed layers under a strong inversion. *Quart. J. Roy. Meteor. Soc.*, **94**, 292–309.
- Lothon, M., F. Couvreux, S. Donier, F. Guichard, P. Lacarrère, D. H. Lenschow, J. Noil-

- han, and F. Saïd, 2007: Impact of coherent eddies on airborne measurements of vertical turbulent fluxes. *Bound.-Layer Meteor.*, **124**, 425–447, doi:10.1007/s10546-007-9182-9.
- Margulis, S. A. and D. Entekhabi, 2001: Feedback between the land surface energy balance and atmospheric boundary layer diagnosed through a model and its adjoint. *J. Hydrometeorol.*, **2**, 599–620.
- McNaughton, K. G. and T. W. Spriggs, 1986: A mixed-layer model for regional evaporation. *Bound.-Layer Meteor.*, **34**, 243–262.
- Miller, M. A. and A. Slingo, 2007: The ARM mobile facility and its first international deployment: measuring radiative flux divergence in West Africa. *Bull. Amer. Meteor. Soc.*, **88**, 1229–1244, doi:10.1175/BAMS-88-8-1229.
- Monteith, J. L., 1965: Evaporation and environment. *Symp. Soc. Exp. Biol.*, **XIX**.
- Noilhan, J. and S. Planton, 1989: A simple parameterization of land surface processes for meteorological models. *Mon. Wea. Rev.*, **117 (3)**, 536–549.
- Paulson, C. A., 1970: The mathematical representation of wind speed and temperature profiles in the unstable atmospheric surface layer. *J. Applied Met.*, **9**, 857–861.
- Ramier, D., et al., 2009: Towards an understanding of coupled physical and biological processes in the cultivated sahel - 1. Energy and water. *J. Hydrology*, **375**, 204 – 216.
- Raupach, M. R., 2000: Equilibrium evaporation and the convective boundary layer. *Bound.-Layer Meteor.*, **96**, 107–141.

- Redelsperger, J. L., C. D. Thorncroft, A. Diedhiou, T. Lebel, D. J. Parker, and J. Polcher, 2006: African monsoon multidisciplinary analysis: An international research project and field campaign. *Bull. Amer. Meteor. Soc.*, **87** (12), 1739–1746.
- Santanello, J. A., M. A. Friedl, and M. B. Ek, 2007: Convective planetary boundary layer interactions with the land surface at diurnal time scales: diagnostics and feedbacks. *J. Hydrometeor.*, **8**, 1082–1097.
- Santanello, J. A., C. D. Peters-Lidard, S. V. Kumar, C. Alonge, and W.-K. Tao, 2009: A modeling and observational framework for diagnosing local land-atmosphere coupling on diurnal time scales. *J. Hydrometeor.*, **10**, 577–599, doi:10.1175/2009JHM1066.1.
- Sellers, P. J., F. G. Hall, G. Asrar, D. E. Strebel, and R. E. Murphy, 1992: An overview of the First International Satellite Land Surface Climatology Project (ISLSCP) Field Experiment (FIFE). *J. Geophys. Res.*, **97**, 18 345–18 371.
- Steeneveld, G. J., B. J. H. van de Wiel, and A. A. M. Holtslag, 2007: Diagnostic equations for the stable boundary layer height: evaluation and dimensional analysis. *J. App. Meteor. Clim.*, **46**, 212–225, doi:10.1175/JAM2454.1.
- Tennekes, H., 1973: A model for the dynamics of the inversion above a convective boundary layer. *J. Atmos. Sci.*, **30**, 558–567.
- van Heerwaarden, C. C., J. Vilà-Guerau de Arellano, A. F. Moene, and A. A. M. Holtslag, 2009: Interactions between dry-air entrainment, surface evaporation and convective boundary layer development. *Quart. J. Roy. Meteor. Soc.*, **135**, 1277–1291, doi:10.1002/qj.431.

Viterbo, P. and A. C. M. Beljaars, 1995: An improved land surface parameterization scheme in the ECMWF model and its validation. *J. Climate*, **8**, 2716–2748.

## List of Tables

- 1 Initial and boundary conditions for model runs of 25 September 2003, Cabauw, The Netherlands and 22 June 2006, Niamey, Niger, without mixed-layer output, which is in Table 2. 39
- 2 Mixed-layer initial and boundary conditions of model runs of 25 September 2003, Cabauw, The Netherlands and 22 June 2006, Niamey, Niger. 40



TABLE 1. Initial and boundary conditions for model runs of 25 September 2003, Cabauw, The Netherlands and 22 June 2006, Niamey, Niger, without mixed-layer output, which is in Table 2.

variable	description and unit	Cabauw	Niamey
$P_0$	surface pressure [Pa]	102900.	98500.
$w_s$	large-scale vertical velocity [ $\text{m s}^{-1}$ ]	0.0	0.0
lat	latitude [deg]	51.97 N	13.48 N
lon	longitude [deg]	4.93 E	2.17 E
doy	day of the year [-]	268.	173.
$w_g$	volumetric water content top soil layer [ $\text{m}^3 \text{m}^{-3}$ ]	0.43	0.198
$w_2$	volumetric water content deeper soil layer [ $\text{m}^3 \text{m}^{-3}$ ]	0.43	0.20
$c_{veg}$	vegetation fraction [-]	0.9	0.2
$T_{soil}$	temperature top soil layer [K]	282.	300.
$T_2$	temperature deeper soil layer [K]	285.	290.
a	Clapp and Hornberger retention curve parameter [-]	0.083	0.219
b	Clapp and Hornberger retention curve parameter [-]	11.4	4.90
p	Clapp and Hornberger retention curve parameter [-]	12.	4.
$CG_{sat}$	saturated soil conductivity for heat [ $\text{K m}^{-2} \text{J}^{-1}$ ]	$3.6 \times 10^{-6}$	$3.56 \times 10^{-6}$
$w_{sat}$	saturated volumetric water content [ $\text{m}^3 \text{m}^{-3}$ ]	0.600	0.472
$w_{fc}$	volumetric water content field capacity [ $\text{m}^3 \text{m}^{-3}$ ]	0.491	0.323
$w_{wilt}$	volumetric water content wilting point [ $\text{m}^3 \text{m}^{-3}$ ]	0.314	0.171
$C1_{sat}$	Coefficient force term moisture [-]	0.342	0.132
$C2_{ref}$	Coefficient restore term moisture [-]	0.3	1.8
LAI	leaf area index of vegetated surface fraction [-]	2.	2.
$r_{c,min}$	minimum resistance transpiration [ $\text{s m}^{-1}$ ]	110.	110.
$r_{s,soil,min}$	minimum resistance soil evaporation [ $\text{s m}^{-1}$ ]	50.	50.
$g_D$	VPD correction factor for surface resistance [-]	0.	0.
$z_{0m}$	roughness length for momentum [m]	0.05	0.05
$z_{0h}$	roughness length for heat and moisture [m]	0.01	0.01
$\alpha$	surface albedo [-]	0.25	0.21
$W_l$	equivalent water layer depth for wet vegetation [m]	$1.4 \times 10^{-4}$	0.0

TABLE 2. Mixed-layer initial and boundary conditions of model runs of 25 September 2003, Cabauw, The Netherlands and 22 June 2006, Niamey, Niger.

variable	description and unit	Cabauw	Niamey
h	initial ABL height [m]	175.	400.
$\theta$	initial mixed-layer potential temperature [K]	284.5	301.2
$\Delta\theta$	initial temperature jump at h [K]	4.2	3.6
$\gamma_\theta$	potential temperature lapse rate [K m <sup>-1</sup> ]	0.0036 <sub><i>h</i>≤950<i>m</i></sub> 0.015 <sub><i>h</i>&gt;950<i>m</i></sub>	0.010 <sub><i>h</i>≤700<i>m</i></sub> 0.0034 <sub><i>h</i>&gt;700<i>m</i></sub>
$A_{\theta_v}$	entrainment ratio virtual potential temperature [-]	0.3	0.18
$adv_\theta$	advection of heat [K s <sup>-1</sup> ]	0.	$f_\theta(t)$
q	initial mixed-layer specific humidity [kg kg <sup>-1</sup> ]	0.0044	0.0138
$\Delta q$	initial specific humidity jump at h [kg kg <sup>-1</sup> ]	-8.0 x 10 <sup>-4</sup>	-0.0044
$\gamma_q$	specific humidity lapse rate [kg kg <sup>-1</sup> m <sup>-1</sup> ]	-1.2 x 10 <sup>-6</sup>	-1.4 x 10 <sup>-6</sup>
$adv_q$	advection of moisture [kg kg <sup>-1</sup> s <sup>-1</sup> ]	0.	$f_q(t)$
u	initial mixed-layer wind speed [m s <sup>-1</sup> ]	5.	5.
$\Delta u$	initial momentum jump at h [m s <sup>-1</sup> ]	3.	0.
$\gamma_u$	free atmosphere wind speed lapse rate [s <sup>-1</sup> ]	0.002	0.001
$\hat{f}_\theta(t)$	-1.0 x 10 <sup>-4</sup> [K s <sup>-1</sup> ] $t_{\leq 11hUTC}$ -1.0 x 10 <sup>-4</sup> $max(1. - 0.36 (t_{hUTC} - 6), -1)$ [K s <sup>-1</sup> ] $t_{> 11hUTC}$		
$\hat{f}_q(t)$	4.17 x 10 <sup>-8</sup> $max(1. - 0.18 (t_{hUTC} - 6), 0)$ [kg kg <sup>-1</sup> s <sup>-1</sup> ] $t_{\leq 11hUTC}$		

## List of Figures

- 1 Overview of the coupled land-atmosphere system and the relevant variables in the daily evolution of evapotranspiration. 43
- 2 Time evolution of boundary-layer height (top left panel), surface heat fluxes (top right panel), potential temperature of the mixed-layer (bottom left panel) and specific humidity of the mixed-layer (bottom right panel) for the Cabauw case. Model is represented by continuous lines, observations by symbols. 44
- 3 Time evolution of boundary-layer height (top left panel), surface heat fluxes (top right panel), potential temperature of the mixed-layer (bottom left panel) and specific humidity of the mixed-layer (bottom right panel) for Niamey. Model is represented by continuous lines, observations by symbols. 45
- 4 Comparison between radiosoundings (thin line) and model results (thick line) for potential temperature (left panel) and specific humidity (right panel) at Niamey. 46
- 5 Contributions to the tendency of the surface evaporation induced by forcings (Cabauw: top left panel, Niamey: top right panel) and feedbacks (Cabauw: bottom left panel, Niamey: bottom right panel). 47
- 6 Contributions of land surface feedbacks to the tendency of the surface evaporation for Cabauw (left panel) and Niamey (right panel). 48
- 7 Time evolution of surface temperature and soil temperature (left panel) and surface resistance and soil volumetric water content (right panel) for both cases. 49

- 8 Contributions to the tendency of the surface evaporation induced by boundary-layer temperature feedbacks (Cabauw: top left panel, Niamey: top right panel) and boundary-layer humidity feedbacks (Cabauw: bottom left panel, Niamey: bottom right panel). 50
- 9 Comparison of the daily range of  $q_{sat}$  in Cabauw (dashed lines) and Niamey (dotted lines) indicated on the Clausius-Clapeyron relationship between absolute temperature and saturated specific humidity. 51
- 10 Contributions of the forcings to the tendency of the surface evaporation for Cabauw (left panel) and Niamey (right panel). 52

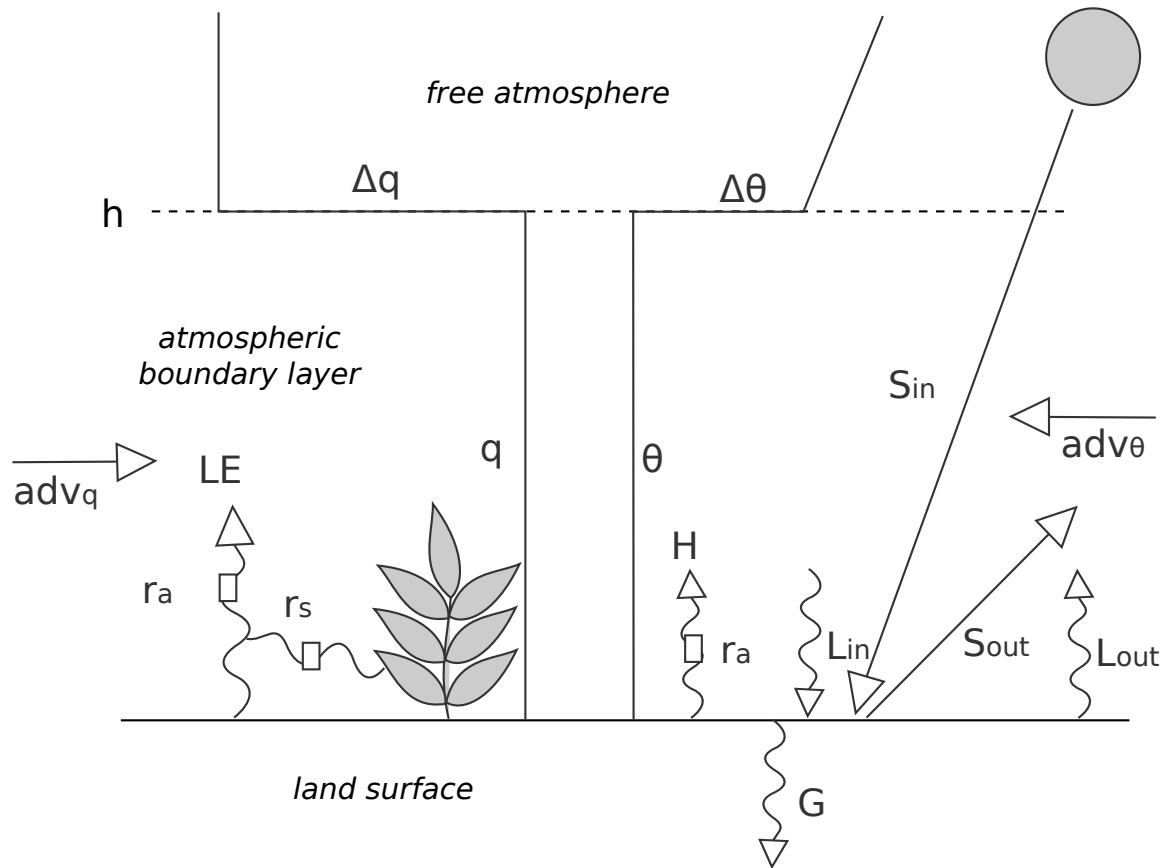


FIG. 1. Overview of the coupled land-atmosphere system and the relevant variables in the daily evolution of evapotranspiration.

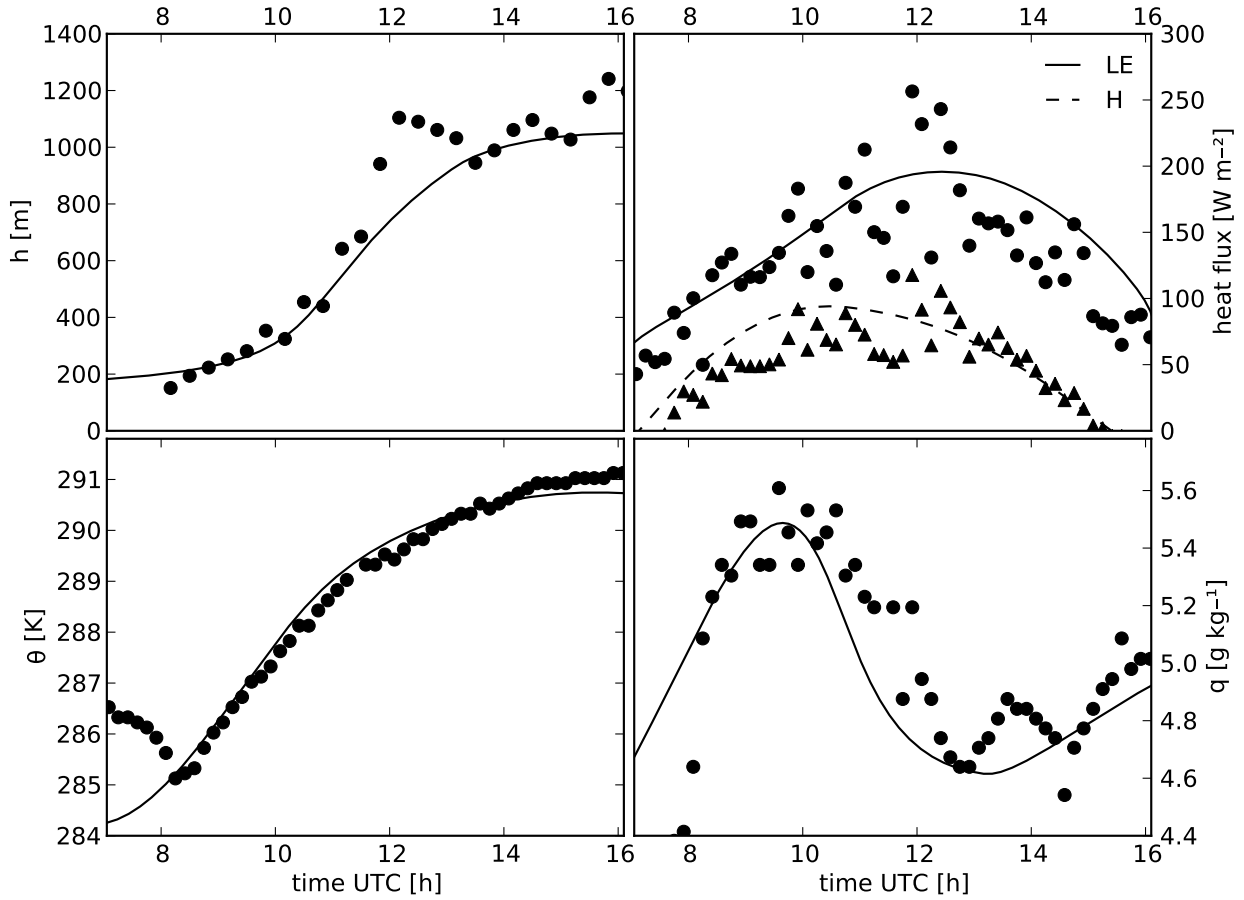


FIG. 2. Time evolution of boundary-layer height (top left panel), surface heat fluxes (top right panel), potential temperature of the mixed-layer (bottom left panel) and specific humidity of the mixed-layer (bottom right panel) for the Cabauw case. Model is represented by continuous lines, observations by symbols.

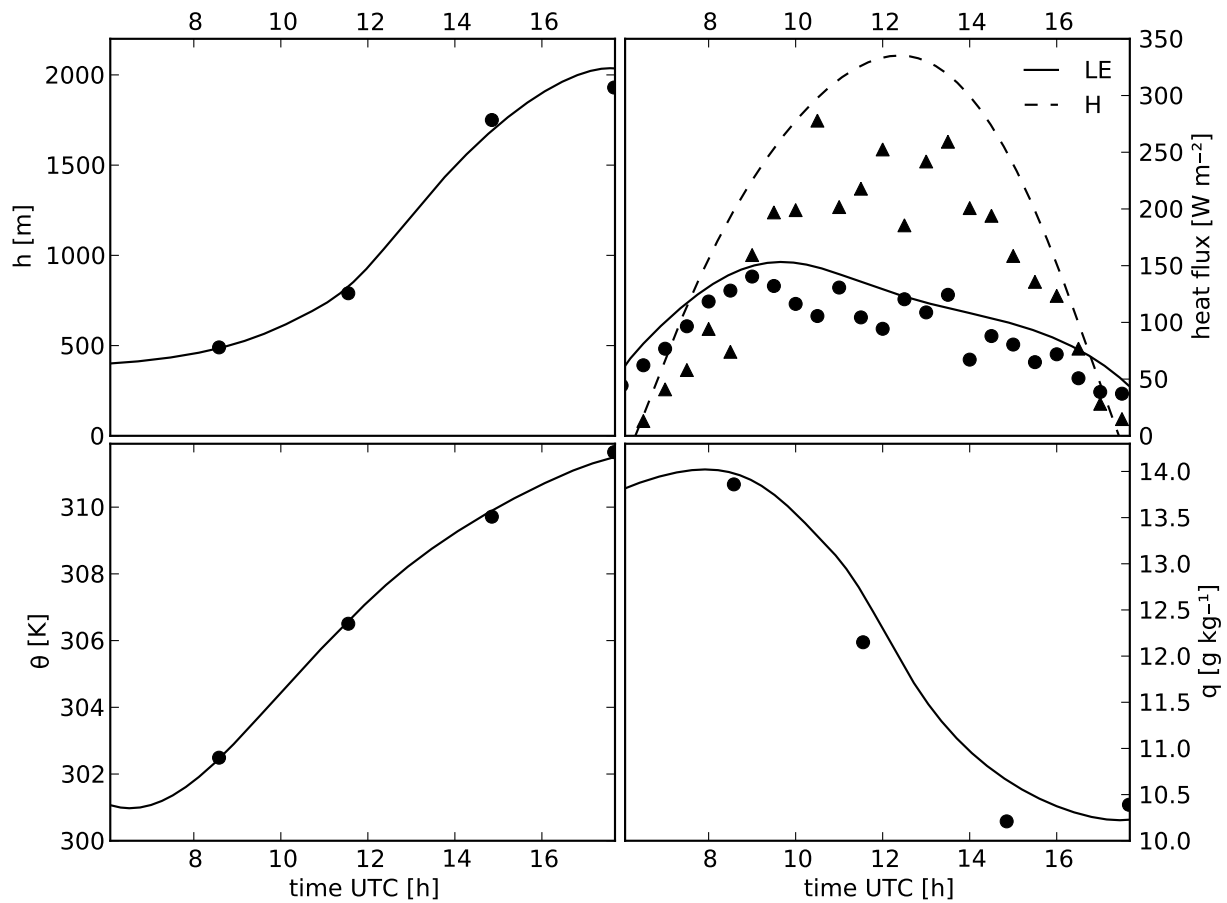


FIG. 3. Time evolution of boundary-layer height (top left panel), surface heat fluxes (top right panel), potential temperature of the mixed-layer (bottom left panel) and specific humidity of the mixed-layer (bottom right panel) for Niamey. Model is represented by continuous lines, observations by symbols.

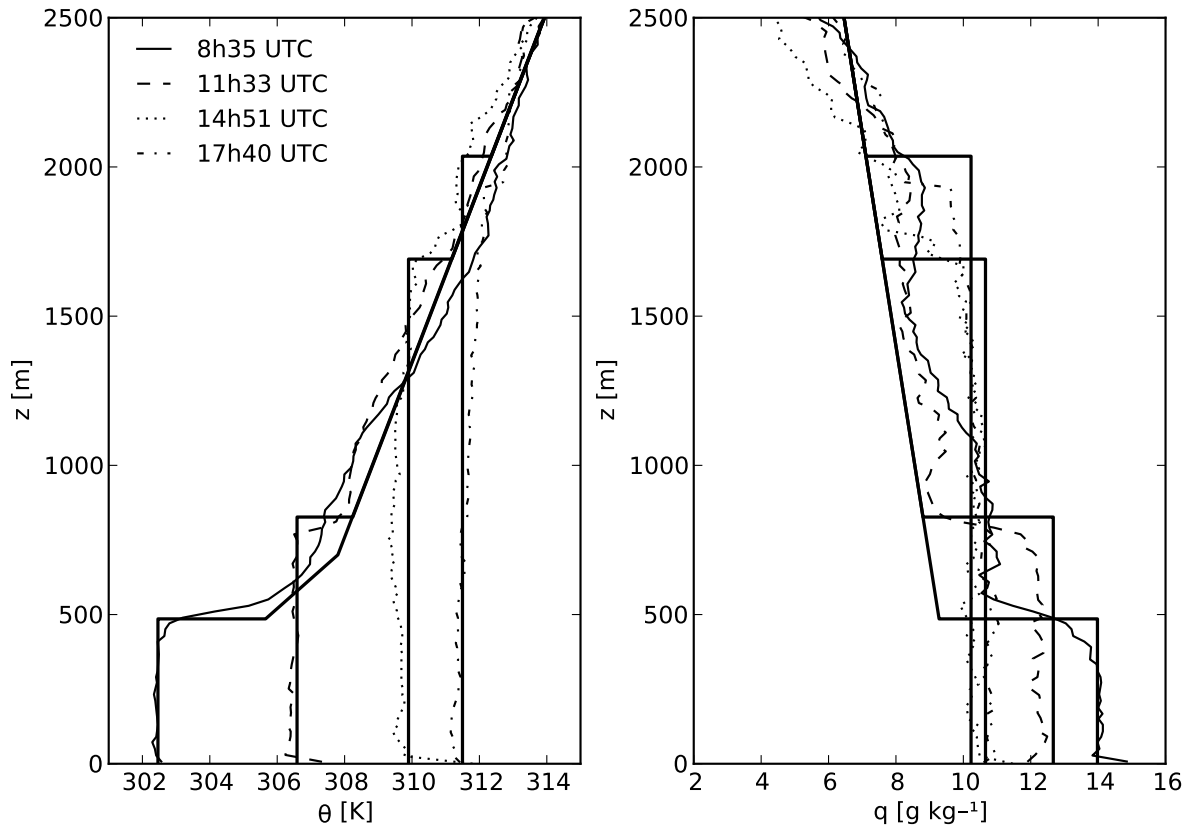


FIG. 4. Comparison between radiosoundings (thin line) and model results (thick line) for potential temperature (left panel) and specific humidity (right panel) at Niamey.



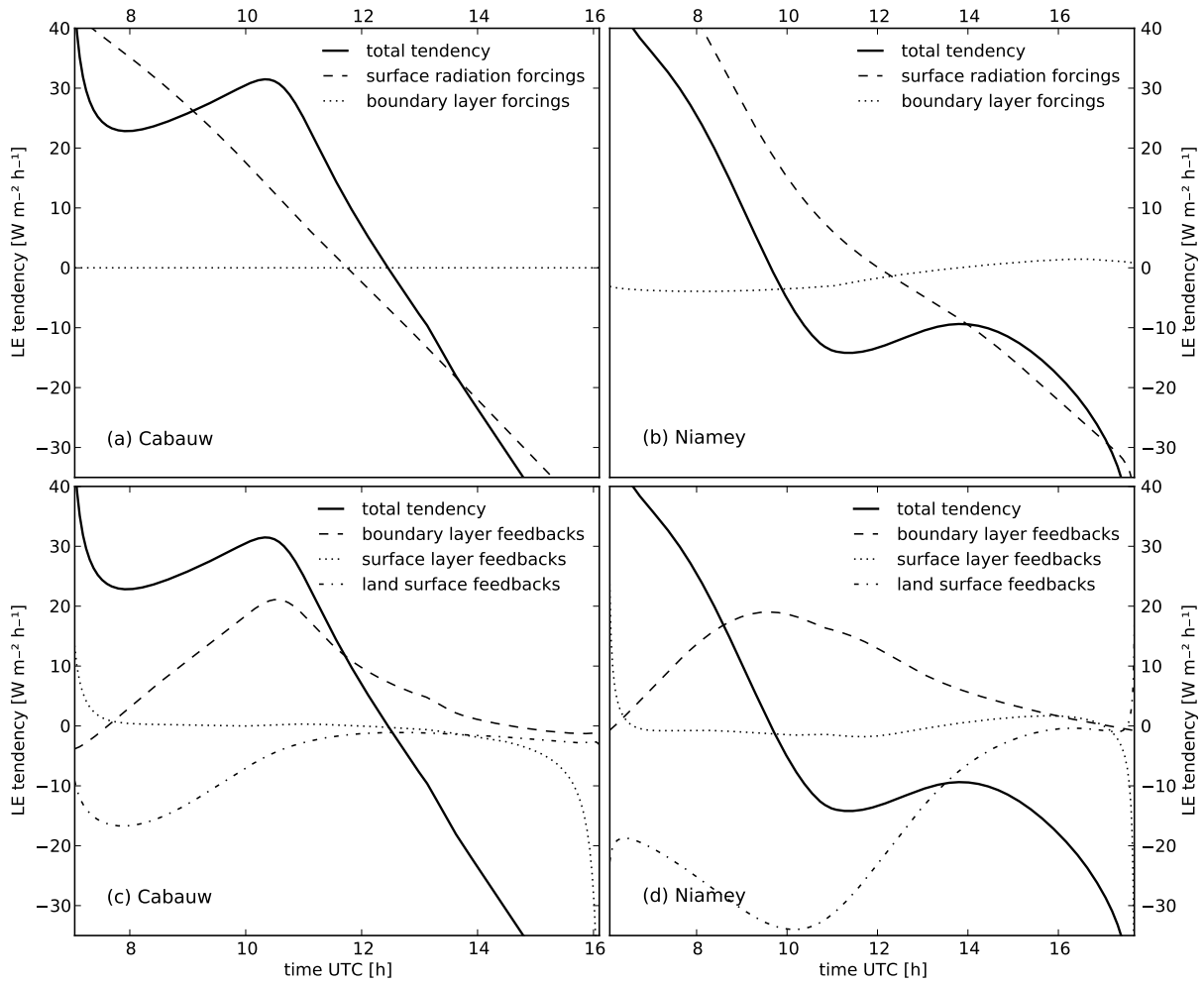


FIG. 5. Contributions to the tendency of the surface evaporation induced by forcings (Cabauw: top left panel, Niamey: top right panel) and feedbacks (Cabauw: bottom left panel, Niamey: bottom right panel).

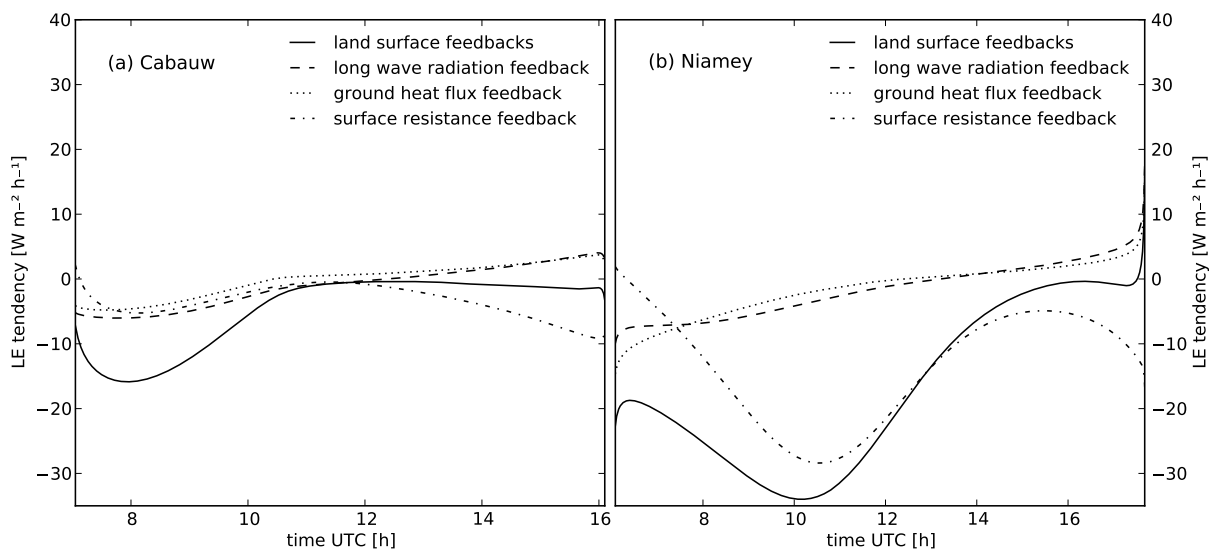


FIG. 6. Contributions of land surface feedbacks to the tendency of the surface evaporation for Cabauw (left panel) and Niamey (right panel).

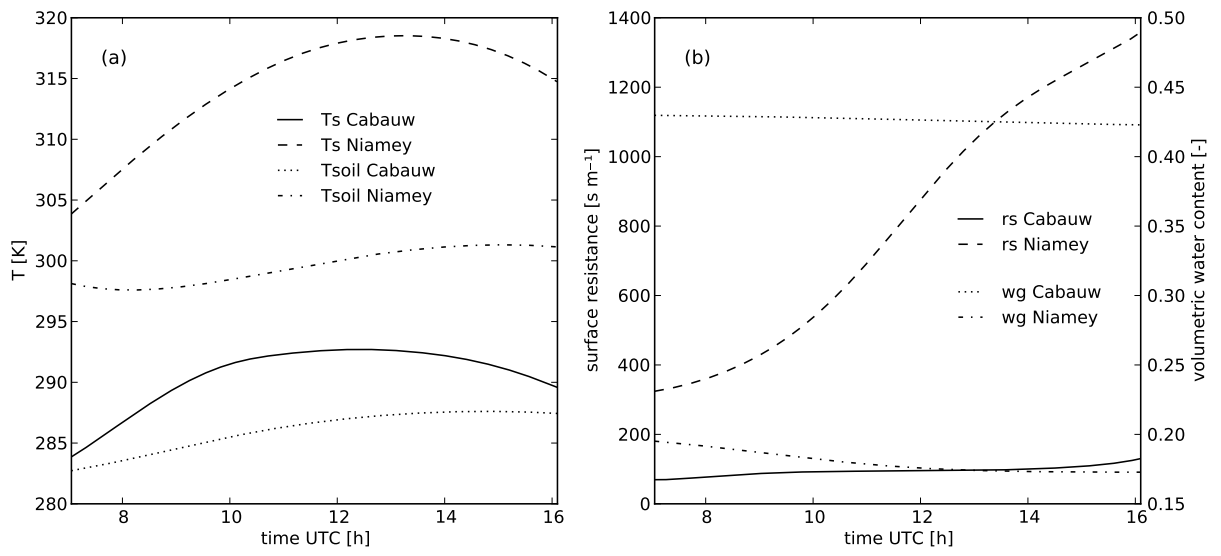


FIG. 7. Time evolution of surface temperature and soil temperature (left panel) and surface resistance and soil volumetric water content (right panel) for both cases.

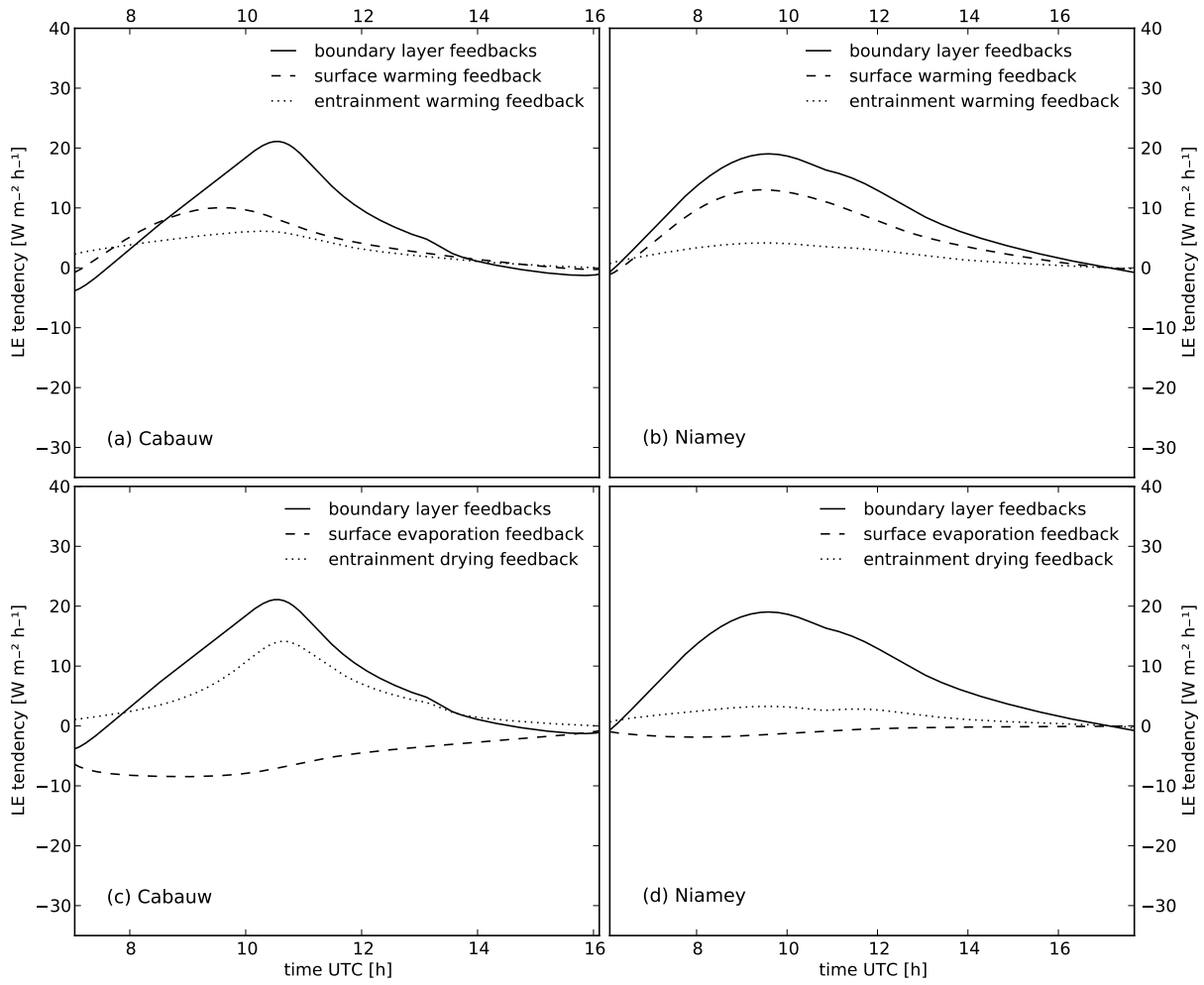


FIG. 8. Contributions to the tendency of the surface evaporation induced by boundary-layer temperature feedbacks (Cabauw: top left panel, Niamey: top right panel) and boundary-layer humidity feedbacks (Cabauw: bottom left panel, Niamey: bottom right panel).

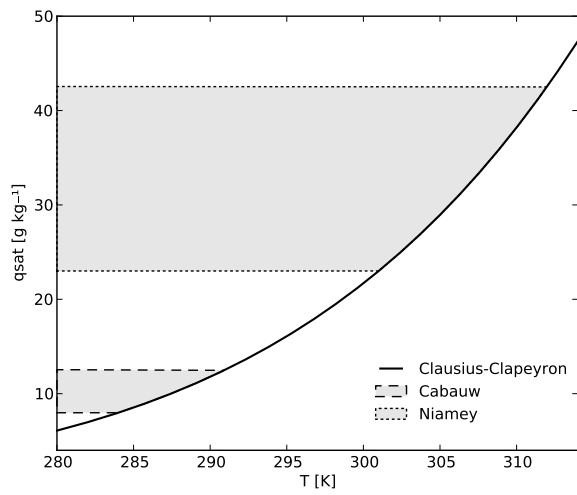


FIG. 9. Comparison of the daily range of  $q_{sat}$  in Cabauw (dashed lines) and Niamey (dotted lines) indicated on the Clausius-Clapeyron relationship between absolute temperature and saturated specific humidity.

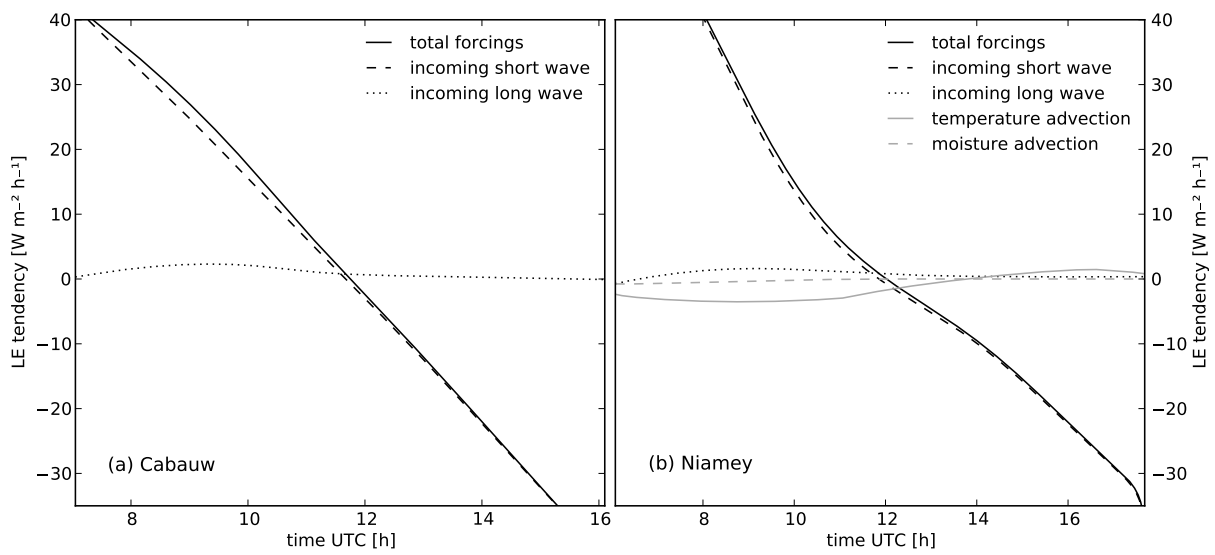


FIG. 10. Contributions of the forcings to the tendency of the surface evaporation for Cabauw (left panel) and Niamey (right panel).